Investigating the influence of deposition techniques and processing conditions on AA2024/SiC FSW joints: Evaluation of microstructural and mechanical properties.

Muhammad Adnan[a], Antonio Barcellona[a], Gianluca Buffa[a*], Davide Campanella[a] and Livan Fratini[a]

[a]Department of Engineering, University of Palermo, viale delle Scienze, 90128 Palermo, Italy

* Corresponding author. tel.: +39-09123861869. *E-mail address:* gianluca.buffa@unipa.it

Abstract

Friction Stir Welding (FSW) has become a mature technology for most metal alloys. The current frontier is the development of in-situ alloyed or reinforced materials to further spread the field of application of this technique. In the paper, SiC-reinforced 2024-T3 aluminum joints were produced by integrating micro-size SiC particles by creating proper features in the sheets. A new joint design was proposed in order to overcome the issues of powder dispersion occurring with the more conventional hole design. The influence of distinct parameters viz., tool rotation speed, traverse speed, and joint configuration on SiC dispersion, microstructure, and mechanical properties of the prepared joints has been corroborated. Standard FSW was also carried out for comparison. The rotation and travel speeds varied ranging 700-1100 rpm and 50- 90 mm/min, respectively. The distribution of reinforcement particles in various zones of the FSW process was examined by using optical microscopy (OM) and scanning electron microscopy (SEM). It was found that the velocity ratio variation influences the heat generation and thereby the microstructural and mechanical properties owing to distinct SiC particulate dispersion throughout the joint area. The welded joints produced at the 1100 rpm and 70 mm/min (S1100-70) combination exhibit an increment in hardness by 30% as compared to base material resulting from grain size reduction and better dispersion of SiC powder. Finally, the analysis of power consumption and temperature during the process was carried out. These additional measurements were crucial in determining the overall performance and feasibility of using SiC powder in the welding process.

Keywords: Friction stir welding, Aluminum alloy, SiC reinforcement, Deposition techniques, Microstructure, Hardness, Tensile properties.

1. Introduction

Aluminum alloy is one of the most important lightweight alloys. It is extensively used in industries such as structural, automotive, and aerospace due to its exceptional characteristics, including high strength relative to its weight, good malleability, high resistance to fracture, strong durability against wear, and excellent protection against corrosion [1]. However, these aluminum alloys have poor weldability, especially for the heat-treatable series. Severe metallurgical challenges arise in fusion welding of aluminum alloys including hot tearing, oxidation, dendritic and eutectic structures, and the creation of hydrogen gas porosity after solidification [2]. To overcome these problems solid-state method i.e. FSW has been demonstrated appropriate for welding several metallic and non-metallic materials, including aluminum alloys. FSW is a solid-state joining technique invented at The Welding Institute (TWI) of UK in 1991 in which the base material does not melt. This technique is particularly favorable for Aluminum alloys since it can be carried out below the melting temperature of the materials [3]. The underlying principle of FSW involves the use of a non-consumable rotating tool characterized by a distinct pin profile and shoulder design [4]. This tool is inserted into the joining edge of two plates and moves at a predetermined traverse velocity. The friction between the rotating tool and the workpiece generates heat which causes plastic deformation and softening of the workpiece while the tool's traverse speed leads to the joining of the workpiece [5-6].

In the aerospace, motorsport, and automotive industries, there has been a significant shift in attention towards reinforced Aluminum matrix composites. This is primarily due to their numerous advantages over conventional base alloys. These composites offer high specific stiffness and strength-to-weight ratio at room temperatures, exceptional fatigue properties, enhanced resistance to wear, and improved formability. However, the main limitation for the industrial applications of reinforced aluminum matrix composite is the inability to use standard fusion welding techniques due to the segregation and

harmful interactions between the reinforcement particles and liquid aluminum in the fusion zone [7]. Thus, FSW is a promising candidate for joining particulate-reinforced aluminum matrix composites because, as a solid-state process, it does not result in brittle solidification products; besides, the energy input and distortion are significantly lower than in fusion welding processes, enhancing the welding aspects [8]. Additionally, through the effect of pinning, dispersed reinforcement particles hinder the growth of grain boundaries during the process of dynamic recrystallization. This mechanism ultimately results in enhanced tensile strength, strain rate, and micro-hardness of the welded materials that have undergone this welding procedure [9].

Recently, several studies investigated the feasibility of FSW on aluminum matrix composite and found that high-quality welds can be successfully produced without defects, with homogenous dispersion of reinforced particles, and improved joint efficiency [10-12]. Dolatkhah et al. [13] investigated the effect of SiC on the microstructure and mechanical properties of 5052 aluminum alloys. Bahrami et al. [14-15] investigated the effect of Nano SiC reinforcement on the improvement of mechanical and microstructural qualities of aluminum alloy 7075. Vidakis et al. [16] have investigated the influence of the Pin design on the mechanical and microstructure properties of the welded joints. Vairis et al. [17] have studied a numerical model comparison between friction stir welding, linear friction, and rotary friction welding. Dewangan et al. [18] investigated the effect of vertical and horizontal zinc interlayers on the material flow by joining dissimilar metal alloys. Buffa et al. [19] have carried out an experimental and numerical campaign of dissimilar lap joints in FSW. The authors found that tool rotation had a larger impact on the joint effectiveness with respect to feed rate. Several researchers have investigated the effect of the number of passes on particle dispersal. Their findings revealed a correlation between the number of passes and enhanced particle dispersion. In other words, as the number of passes increases, the distribution of particles becomes more uniform [16-19].

A few studies have been conducted to evaluate the influence of tool rotational speed to traverse speed on the mechanical and microstructure aspects of welded joints [20-22]. Zohoor et al. [23] investigated the effect of reinforced particle size on the mechanical and microstructural properties by using both nano and micro-size reinforced particles. Previous studies have been conducted based on the fabrications of metal matrix composite (MMC) using various deposition methods, such as drilled holes method [24] groove method [25-26] and direct pasting [27]. The way in which reinforced particles are deposited plays a crucial role in ensuring that the resulting material is consistent, uniform, and can be evenly spread throughout. This deposition process can have a significant impact on the physical properties of the material, especially when it comes to the way in which the properties change across the material's structure [28]. Achieving a uniform dispersion of reinforced particles (RPs) during the process with a defect-free outcome is a challenging issue. This is due to the asymmetric flow of material, which can be minimized by using multiple passes or by altering the rotation of the tool during the process.

Based on the literature review presented, it arises that the techniques currently used have several restrictions, such as the reinforced particles scattering out or gathering in the rupture as the number of passes increases, resulting in only a small number of reinforced particles being actually embedded in the joint.

With respect to these limitations, a new deposition strategy is proposed, in which a slurry of reinforced particles SiC is placed inside a slot embedded on the adjoining faces of 2024-T3 aluminum alloy sheets. The final aim is to reduce the ejection of reinforced particles from the joints interface and improve their dispersion uniformity. A comparison is made between the proposed approach and both the more conventional "hole on plates" method and no powder joints. The study investigates the impact of the sheets configuration, rotational speeds, and traversal speeds on the microstructure, hardness, and tensile behavior of FSWed joints. Finally, the power consumption is investigated to assess the proposed approach sustainability with respect to conventional FSW.

2. Materials and experimental procedure

2.1 Materials

In this research, AA2024-T3 Aluminum alloy sheets with dimensions of 120 mm × 70 mm × 5 mm were employed as base material. The chemical composition and mechanical properties are listed in Table 1 and Table 2, respectively. SiC powder with an average particle size of 5 µm and a purity of 99.9% was utilized as the reinforcement. The density of the SiC powder used in the experiment was 3.31 g/cm^3.

Table. 1 Chemical composition of AA2024-T3.

Cu	Mg	Mn	Si	Zn	Al
3.6	1.45	0.45	0.06	0.05	Bal.

Table. 2 Physical properties of AA2024-T3[29].

Tensile strength, MPa	Yield stress, MPa	Elongation, (d, %)	Poisson's ratio	Young's modulus, GPa	Density g/cm^3
450	315	0.18	0.33	73.1	2.78

2.2 Experimental Procedure

Experimental tests were conducted on the ESAB LEGIO FSW Machine. The FSW machine and fixture are shown in Figure 1. In Figure 2.a and b, the 3D drawing, and image of

the welding tool used in the experimentation process are presented. The tool was made of H13 tool steel.
The tool shoulder had a diameter of 16 mm, and the tapered pin had diameters of 5 mm and 3 mm at the top and bottom, respectively. The height of the pin was 2.7 mm. The tool plunge depth is 3 mm. The tilt angle used during the process is 2.5º.

Fig. 1. (a) ESAB Legio 3 ST machine for FSW (b) The machine's enclosure and Multimeter for the measurements exhibited both current clamps and tension alligator clips. (c) Fixture layout for the FSW process and K-type thermocouple.

Two strategies were considered to incorporate the powder into the sheets before the process. The first strategy involved a peculiar sheets edge design, as depicted in Figure 2a. A slot was milled in the two sheets so that when in contact, a channel is left all along the separation surface. In this way, the microparticles were fully contained within the workpieces during the welding process. The design entailed making a 1 mm high protrusion in the Al plate and a 2 mm deep groove in the Aluminum plate, as shown in Figure 2 (a). When the workpieces are joined, an embedded square “channel”, with a side of 1 mm, is obtained between the plates. This design prevented any dissipation of SiC powder during the welding process. The second strategy involved a more conventional sheet design, having 34 cylindrical holes drilled at the adjoining edges, with 17 holes per sheet. This approach, which usually involves some powder dispersion during the process, was used to evaluate the performance of the proposed unique groove design. The holes had a diameter of 2 mm and a depth of 2.5 mm (Figure 2 (b)). In order to determine the effect of reinforced powder on the mechanical and microstructural properties of the joints, simple plates were welded without powder. All the aluminum plates were cut to size and then scrubbed with a stainless-steel brush to remove surface oxide deposits. Subsequently, high-purity acetone was used to clean the surfaces. To fill the grooves and hole with SiC, a thick slurry of SiC and 99% pure ethanol was prepared, while the slot and hole were cleaned with acetone beforehand to prevent contamination. Once cleaned, the SiC mixture was poured into the grooves and hole plates, and then left to dry for 30 minutes at room temperature.

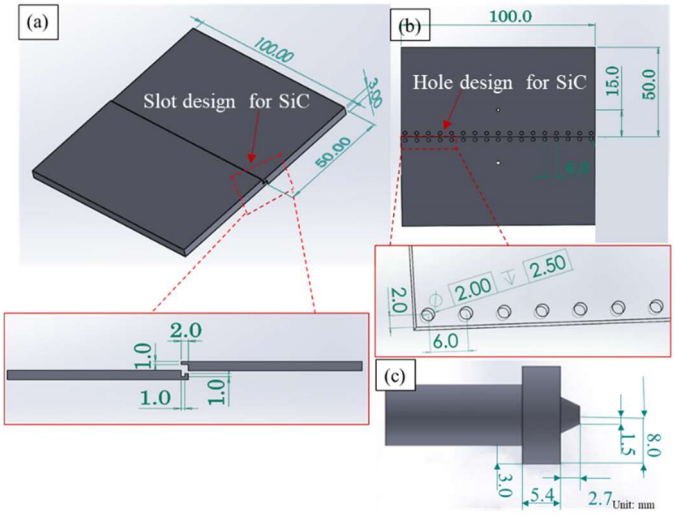

Fig. 2. (a) Slot design applied to incorporate the reinforced particles into the joint's surface. (b) Hole design plates to embed the reinforced particles into the joint. (c) Dimensions of FSW tools used.

Fluke 435 power quality analyzer which is commercially available and capable of capturing the voltage, current, and power history, was utilized to conduct the energy measurements. The dedicated multimeter for power consumption is shown in Figure 1 (b). The temperature was observed using two thermocouples of K-type placed at different weld lengths 15 mm away from the welding line on the advancing side, as shown in Figure 1 (c). These thermocouples were beaded at the tip and adhered in place with a high-temperature chemical cement, 1 mm below the upper layer of the sheet. Temperature data were recorded at a sampling rate of 1 Hz.

Table 3 Combinations of processing parameters.

Specimen No	Tool rotation speed (RPM)	Tool traverse speed (mm/mint)	Velocity Ratio (VR)
S700-50	700	50	14
S900-50	900	50	18
S1100-50	1100	50	22
S700-70	700	70	10
S900-70	900	70	13
S1100-70	1100	70	16
S700-90	700	90	8
S900-90	900	90	10
S1100-90	1100	90	12

The combination of process parameters such as tool rotational speed (RS), traverse speed (TS), and the resulting velocity ratio (VR) are shown in Table 3. All the case studies have been carried out with three passes in order to increase the dispersion of the SiC powder, based on previous observations

of some of the authors [30]. To evaluate the mechanical properties of the FSWed joints at room temperature, uniaxial tensile tests were conducted. These tests were carried out on a servo-hydraulic testing machine, with specimens cut from the joints in such a way that the loading direction was perpendicular to the welding line. The cutting position was chosen to be in the dip or hump zones, with the gauge width matching the shoulder mark. The tensile test specimens were made according to the ASTM-E8 standards. Engineering stress (s) versus engineering strain (e) data were collected and analyzed, specifically focusing on determining the ultimate tensile strength (UTS). Each process condition was tested three times.

The hardness profile of the samples was measured using a Vickers micro-hardness tester. A 1000 gm load was applied for a dwell time of 10 seconds while maintaining a 1 mm gap between indentations. Prior to the test, the samples were meticulously polished using emery papers graded between 80 and 1200. The indentations were made on the cross-section surface, specifically 1.5 mm below the top surface. For microstructural examination, samples measuring 15 × 3 × 3 mm were utilized. The examining surface underwent polishing with papers graded between 6 and 1 micron, followed by super polishing using ¼ micron-grade paste. To investigate the microstructure, the polished samples were etched with a solution of caustic soda (10% NaOH + 90% water) for approximately 30 seconds. Grain size measurement was conducted using the ImageJ software at 100x resolution. Microstructure analysis utilized an optical microscope (Model: Olympus GX-51-100X). The compositional elements were examined through Scanning electron microscopy (SEM) acquired by Phenom ProX Desktop and energy dispersive spectroscopy (EDS) Zeiss, Model: Ultra-55 SEM.

3. Results and Discussion

3.1 Weld Surface Appearance

Optimal weld quality, displaying few defects, was achieved when the rotation speed ranged from 700 to 1100 rpm and the travel speed ranged from 50 to 90 mm/min. However, deviations from this range resulted in non-uniform surfaces and the formation of defects such as cracks, cavities, and tunnels. In more extreme scenarios involving high rotation and travel speeds, FSW joints exhibited failure with cracking along the interface and fracture surfaces. The welded surface appearances without powder at three passes in selected FSW samples can be observed in Figure 3. The heat generated was insufficient at the beginning of the process for sample S700-90, as can be seen from the cracks at the beginning and at the end of the weld seam, while the weld quality improved for sample S1100-70 due to a decrease in travel speed. Increasing the rotation speed resulted in defects for the sample S1100-50, likely due to localized melting and liquation in the SZ. The high level of heat generated during FSW led to hot crack development during cooling, resulting in defective weld joints. The surface appearance of the weld does not change with the addition of the powder in 3 passes both in slot and hole design.

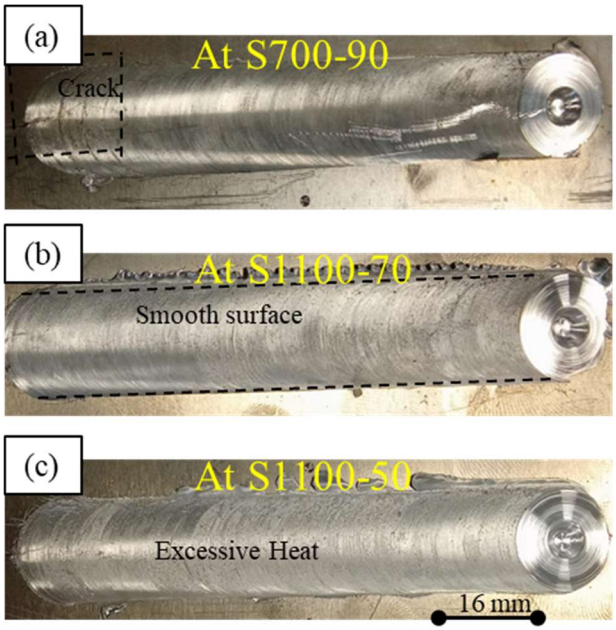

Fig. 3. Surface appearance of the friction stir weld sample without powder at three passes (a) S700-90 (b) S1100-70 (c) S1100-50.

3.2 Metallurgical observations

3.2.1. Macrostructure

In FSW of MMC joints, there are two primary factors that impact the strength of the resulting weld joints. These factors include macro-features, such as defects in the form of cavities or tunnels, and micro-features, specifically the formation of intermetallic compounds within the stir zone. Both factors can have a significant impact on the overall quality and durability of the weld joint. The macrostructures of all three different kinds of welded joints are shown in Figure 4. Based on Figure 4 (a), sample S700-70 without powder and three passes, it appears that a low rotation speed did not generate sufficient heat to allow for proper material flow during the welding process. As a result, various defects such as micro-voids, cavities, and micro-cracks were observed in the stir zone. Figure 4 (b), showing the S700-90 case study without powder, reveals that maintaining constant rotational speed while increasing the traverse speed leads to a higher rate of heating, causing more defects such as cracks and cavities. Increasing the rotation speed during welding results in higher heat generation and plastic deformation. This leads to the stir zone becoming smaller and more spherical in shape. At high rotational and traverse speeds, an excessively high level of heat input can negatively affect the overall quality of the weld joint. This is evident from the uneven surface appearance observed in Figure 4 (c), which highlights the detrimental effects of excessive heat input obtained for the sample S1100-90 without powder and three passes case study. Figure 4(d) illustrates the sample S1100-70 case study after three passes without powder, demonstrating the successful creation of defect-free joints. Apparently, no defect or cavity has been observed. The effect of the plate design such as hole and slot design on the macrostructure of the welded joints has been observed for the same process parameters and three passes. Figure 4 (e), (f) showing the sample S1100-70 having hole and slot design

plates welded joints respectively. It reveals that at optimum process parameters on sample S1100-70 defect-free welded joints have been produced on all three welded joints. However, at some points, agglomeration of SiC powder has been observed which can be attributed to inadequate consolidation and insufficient material flow in the weld nugget zone.

Following the FSW process, distinct regions are formed within the weld joint, such as SZ, TMAZ, and HAZ [29]. The size and shape of the nugget zone are subject to variations based on different process parameters, including factors such as tool design, workpiece temperature, and the thermal conductivity of the material. By increasing the number of passes and heat input, defects like micro-voids and interface micro-cracks reduce in size. In Figure 4 The satisfactory material flow around the tool pin is evident in the macrostructure of the defect-free samples.

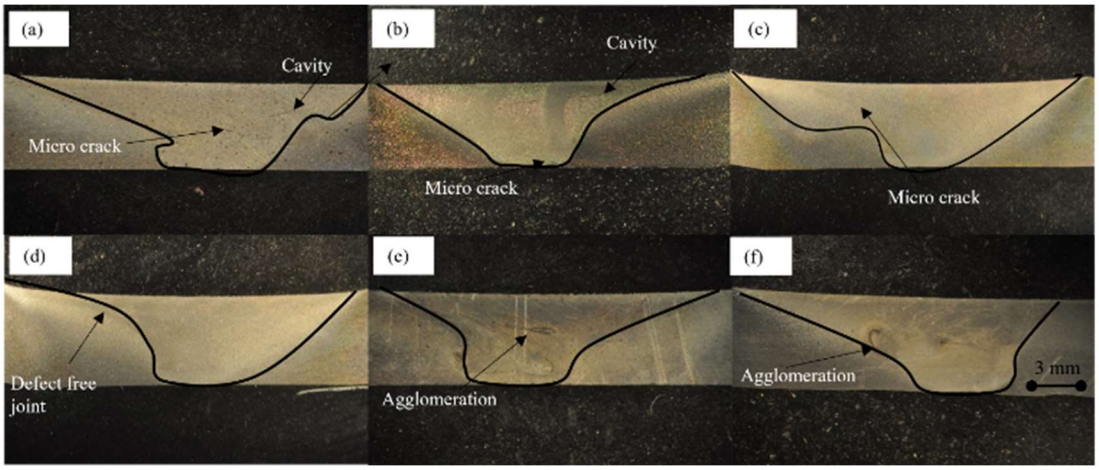

Fig. 4. The effect of process parameters on the welded joints after three passes. (a) S700-70-without powder. (b)S700-90-without powder. (c) S1100-90-without powder. (d) S1100-70-without powder. (e). S1100-70 with powder hole design welded joints. (f) S1100-70 with powder slot design welded joints.

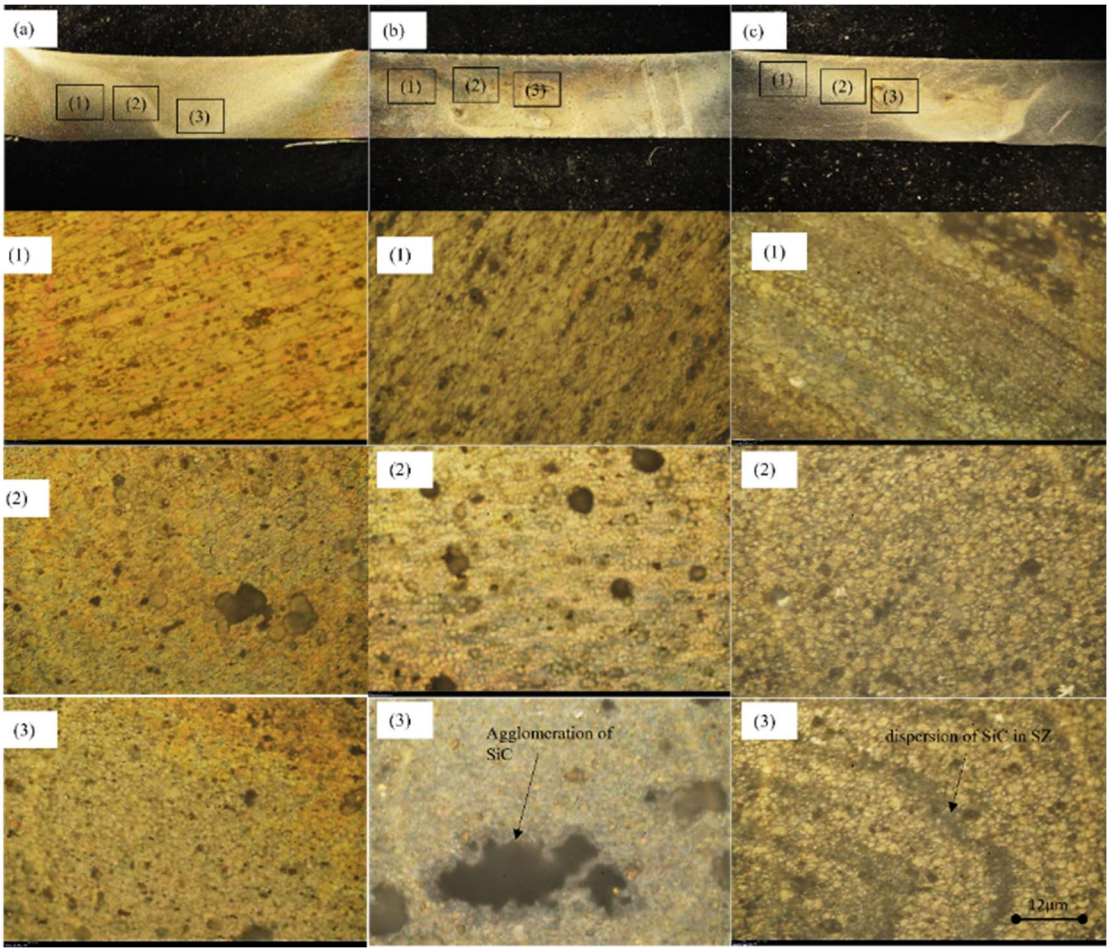

Fig. 5. Microstructure image of the sample at different zone. (a) Sectional macrostructure Diagram of FSW sample S1100-70-without powder. (b) Sectional macrostructure Diagram of FSW sample S1100-70-hole plate. (c) Sectional macrostructure Diagram of FSW sample S1100-70-slot plate.

3.2.2. Microstructure analysis

Microstructure analyses have been performed on the hole plates, slot plates, and without powder specimens. Microstructure analysis of three distinct plate designs under S1100-70 parameters is depicted in Figure 5. In this configuration, the joint nugget experiences significant plastic deformation at elevated temperatures, causing dynamic recrystallization (DRX) to occur. Consequently, fine recrystallized grains form, exhibiting notable differences from the grains present in the original materials. Figure 5 (a,b,c) shows the microstructure of the stir zone. The microstructure of the SZ in the hole plates and slot plates reveals a finer grain size due to dynamic recrystallization, while the TMAZ exhibits coarser grains since DRX does not occur in that region. Reinforcement nanoparticles play a crucial role in hindering grain boundary motion, limiting grain growth through the pinning effect, and increasing nucleation sites. The presence of these particles also results in the fragmentation of original grains, leading to a substantial reduction in grain size compared to weld samples that lack microparticles. Consequently, the inclusion of these reinforcements enhances the strength and toughness of the weld joint. When comparing the hole and slot specimen with the ones produced without powder, the grain size is higher. It can be observed that at consistent traverse speed, the grains in the material become larger when the heat input increases, i.e. rotation speed increases and/or travel speed rate decreases. Higher heat input has a dual impact on the microstructure. It can reduce the impact of annealing and recrystallization, but it can also cause SiC particle accumulation and agglomeration, which reduces the refining effect. As a result, more grain growth occurs. In this way, the finest grain size has been observed for process parameters resulting in proper temperature, as it will be shown in the following. The pinning effect caused by the addition of SiC and 3P results in a decrease in grain size. The average grain size in the slot plate and hole plates was reduced to 2.5 µm which is much lower than the base material grain size. The average grain size in the plate without powder is 3.5 µm, which is slightly higher than slot and hole plate shown in Figure 6. The grain size reduction observed for without powder welded joints is due to the number of passes. In fact, increasing the number of passes results in finer grain in the stir zone.

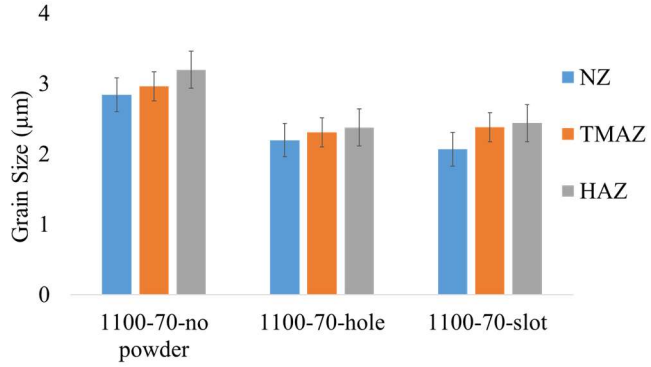

Fig. 6. Sectional Average Grain Size comparison at S1100-70 hole, slot, and without powder.

In order to understand the effect of process parameters and plate design on the dispersion of micro-sized SiC in the stir zone, SEM analyses have been performed. Figure 7 shows the SEM analysis for various process parameters. In Figure 7 (a) at S1100-70- slot design, it can be observed that with a SiC content in the slot, a homogeneous distribution of particles with significant fragmentation was observed. The absence of particle clustering indicates a strong bond between the particles and the aluminum matrix. The presence of small-sized SiC particles hinders the movement of grain boundaries and limits grain growth by causing a pinning effect [28]. This effect leads to a reduction in grain size Additionally, it is evident that the SiC particles are strongly bonded with the aluminum matrix. Figure 7 (b) shows the bonding between SiC and base metal. Figure 7 (d), (e) at S1100-70-hole design shows the homogenous dispersion of SiC in the stir zone. There is a perfect bonding between SiC and aluminum 2024-T3. It can also be observed in slot design the percentage of SiC is more than in hole design. In order to observe the effect of process parameters on the dispersion of SiC Figure 7(g), (h) shows that at S700-50 there is evidence of agglomeration of SiC particles along with inadequate bonding with the aluminum metal matrix. The agglomeration of particles indicates insufficient material blending caused by low heat input at lower rotational speeds. Insufficient heat input at lower rotational speeds (RS) results in inadequate material flow. This leads to the aluminum metal matrix becoming highly viscous in the weld zone (SZ), causing unconventional material mixing. Hence, sufficient heat is necessary to ensure effective material flow, resulting in the uniform dispersion of reinforcement particles in the weld zone through increased stirring action at higher rotational speeds. Figure 7 (j), (k) at S1100-90 i.e., at high rotational and traverse speed, also shows the agglomeration at some parts and insufficient bonding between SiC and aluminum metal matrix due to excessive heat produced during the process.

Figure 7 (c), (f), (i), (l) shows the Energy-Dispersive X-ray Spectroscopy (EDS) in order to see the percentage of reinforced particle dispersion. It is observed that in slot plates the percentage of SiC is higher than that in the hole plate. All of these experiments have been done on three passes, as the increase in the number of passes results in more uniform dispersion.

3.3. Mechanical properties

3.3.1. Tensile strength

It was observed that the welded joints failed at the joining interface and boundary of the TMAZ and the SZ. This area includes intermetallic compound (IMC) layers and welding defects such as interface cracks, cavities, and tunnels. From the graph, it is shown that the overall tensile strength of plates without powder at three passes is higher than the welded joints containing SiC, i.e. hole plates welded joints or slot plates welded joints. The highest UTS achieved without SiC is 385 MPa, which is 85% of the 2024-T3 aluminum base material shown in Figure 8. On the other hand, the tensile stress obtained with SiC powder is comparatively lower than without powder. The maximum tensile strength at the hole plate and slot plate is 338 MPa and 280 MPa while their efficiencies are 75 % and 62 % respectively. The reduction of tensile strength with powder

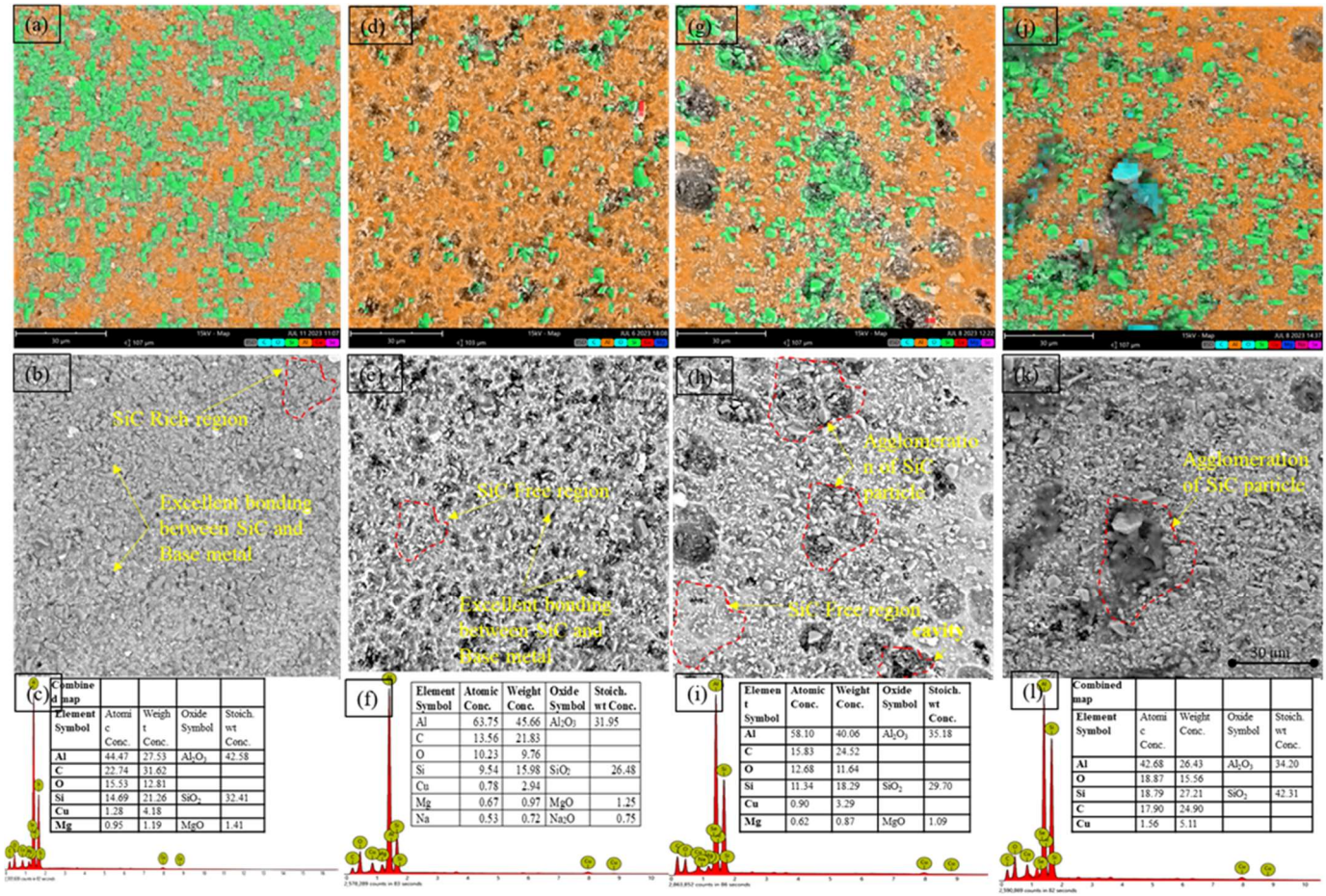

Combined map				
Element Symbol	Atomic Conc.	Weight Conc.	Oxide Symbol	Stoich. wt Conc.
Al	44.47	27.53	Al_2O_3	42.58
C	22.74	31.62		
O	15.53	12.81		
Si	14.69	21.26	SiO_2	32.41
Cu	1.28	4.18		
Mg	0.95	1.19	MgO	1.41

Element Symbol	Atomic Conc.	Weight Conc.	Oxide Symbol	Stoich. wt Conc.
Al	63.75	45.66	Al_2O_3	31.95
C	13.56	21.83		
O	10.23	9.76		
Si	9.54	15.98	SiO_2	26.48
Cu	0.78	2.94		
Mg	0.67	0.97	MgO	1.25
Na	0.53	0.72	Na_2O	0.75

Element Symbol	Atomic Conc.	Weight Conc.	Oxide Symbol	Stoich. wt Conc.
Al	58.10	40.06	Al_2O_3	35.18
C	15.83	24.52		
O	12.68	11.64		
Si	11.34	18.29	SiO_2	29.70
Cu	0.90	3.29		
Mg	0.62	0.87	MgO	1.09

Combined map				
Element Symbol	Atomic Conc.	Weight Conc.	Oxide Symbol	Stoich. wt Conc.
Al	42.68	26.43	Al_2O_3	34.20
O	18.87	15.56		
Si	18.79	27.21	SiO_2	42.31
C	17.90	24.90		
Cu	1.56	5.11		

Fig. 7. SEM micrographs reveal the dispersion of SiC in the SZ: (a) at S1100-70- slot mapping (b) at S1100-70- slot dispersion (c) EDS composition analysis region at S1100-70-slot (d) at S1100-70- hole mapping (e) at S1100-70- hole dispersion (f) EDS composition analysis region at S1100-70-hole (g) at S700-50-slot mapping (h) at S700-50- slot dispersion (i) EDS composition analysis region at 700-50-slot (j) at S1100-90-slot mapping (k) at S1100-90- slot dispersion (l) EDS composition analysis region at 1100-90-slot.

is due to the agglomeration of reinforced powder, porosity effect, microvoids, and intermetallic compounds. From the graph, it was observed that tensile strength increased with the increment of the heat input at a certain level. At sample 1100-70 having a medium heat index, more homogenous SiC dispersion has been reached in the stir zone and the maximum tensile strength has been observed. By increasing the heat index results in agglomeration of SiC which, in turn, causes a decrease in tensile strength. Sample S700-90 shows the lowest tensile strength for all three configurations. These joints are characterized by low HI and incomplete intermixing of materials together with the presence of cracks and cavities. These factors reduce the effective working area, promote stress concentration, and ultimately decrease the joint's ability to tolerate tension stress. This drawback can outweigh the advantages of refining the grain structure and hinder the ability of the welded joint to attain the desired strength and elongation. Tensile testing has revealed that specimens formed through FSW demonstrate brittle characteristics and have decreased ultimate tensile strength when compared to the parent materials. From the above considerations, it arises the existence of proper process parameters.

3.3.2. Microhardness

The addition of reinforcement particles increases the hardness level in two different ways.

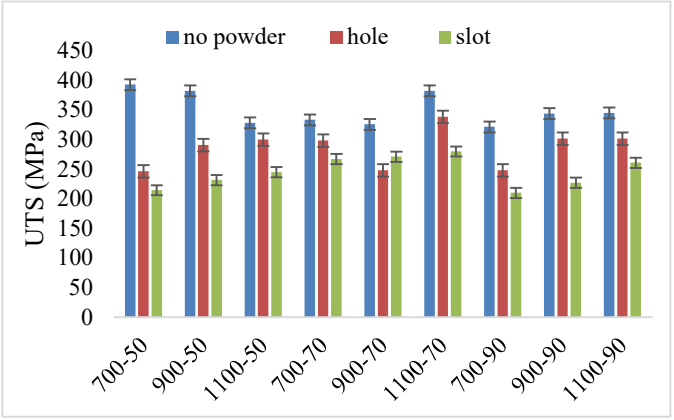

Fig. 8. UTS Comparison at various process parameters.

Firstly, they aid in reducing the grain size which results in higher hardness levels. Additionally, the reinforcement particles themselves are inherently ultra-hard and are present in an agglomerated form. This further contributes to the overall hardness level of the material. The distribution of hardness in the SZ is typically not uniform, and it can be affected by various factors. These factors include the formation of different phases, the extent of recrystallization that leads to the creation of very fine grains, and an increase in the density of dislocations. The higher rotation speed of the tool can result in

a larger dislocation density, which can lead to increased hardness. In addition, the presence of hard and brittle IMCs can cause severe peaks in hardness. The amount of IMCs also affects the hardness. The difference in hardness throughout the SZ can also be attributed to the presence of intercalated banded structures.

The Microhardness of the three welded profiles, namely hole plates, slot plates, and simple plates at the best performing process parameter, as resulting from the previous analyses, are shown in Figure 9. The maximum hardness value is 178 HV which is 30% higher than the hardness of the base material in the slot plate welded joints. The hardness value is maximum in the stir zone as the maximum grain refinement occurs in this area. There exists an inverse relationship between grain size and hardness, meaning that as the grain size decreases, the hardness value increases. The SiC particles have a significant impact on the hardness due to their high hardness and resistance to plastic deformation during indentation, resulting in an overall increase in hardness. The area with low hardness such as at the start and end point of the welded region can be related to the SiC-free region and non-recrystallized grains. It is observed that for the hole plates welded joints the hardness is comparatively lower than slot plates. The reason could be that the amount of reinforced particles is comparatively lower than the one used in the slot plates. In the stir zone, as the number of passes increases, the grains are comparatively smaller in size than the base metal, so an increment of hardness has been observed. Finally, as process parameters are regarded, hardness values increase with increasing n rotational speed. However, when the HI is too high, the scattering of SiC particles causes a reduction in hardness value.

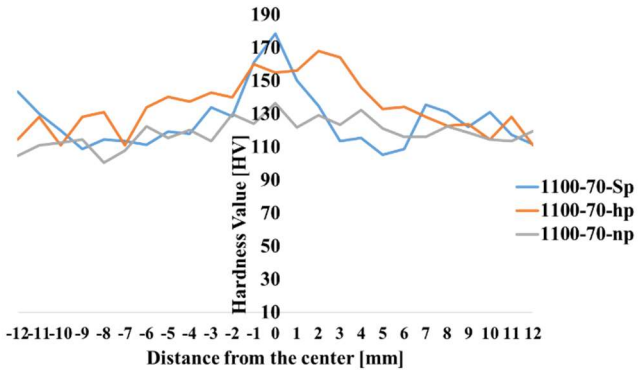

Fig. 9. Average hardness value compared to the distance from the centre of the weld.

3.4 Temperature distribution

In FSW, the rotating tool and the workpieces experience intense plastic deformation and friction. Both of these factors play a role in the temperature increase within the stir zone during the welding process. The dissipation of heat is vital in determining the weld's quality. If the frictional heat generated around the centerline is insufficient, it can hinder the lateral movement of the tool, potentially causing tool pin breakage. Conversely, higher frictional heat and resulting temperatures can improve the flow of metal, resulting in smoother transverse movement of the tool. However, excessively high temperatures can cause the material to stick to the pin and shoulder, as well as to excessive grain growth, leading to a larger microstructure grain size. In this study, temperature has been recorded for all the 3 passes to observe the difference in temperature due to the passes and the powder distribution (Figure 10). Results show that temperature increases with the increase in the number of passes in reinforced welded joints. The reason is that with the passage of the tool, the dispersion of the reinforced powder becomes more uniform and the friction between the tool and SIC powder generates more heat. From the graph, the temperature on the advancing side is higher than the temperature on the retreating side of the welded plates. Figure 10 (a) shows the maximum temperature comparison for the 1100-70 case study obtained with the three different configurations. From the results, it is seen that temperature increases continuously in slot and hole plates with the number of passes while, for simple plates, there is not any significant increase in temperature with the number of passes. This is because reinforced powder leads to an increment in the temperature when the dispersion becomes more uniform. The temperature also increases with the increase in HI, i.e. increase in tool rotation and/or decrease in feed rate. Figure 10 (b) shows the temperature history recorded for the case study characterized by S1100-70 slot design for all three passes.

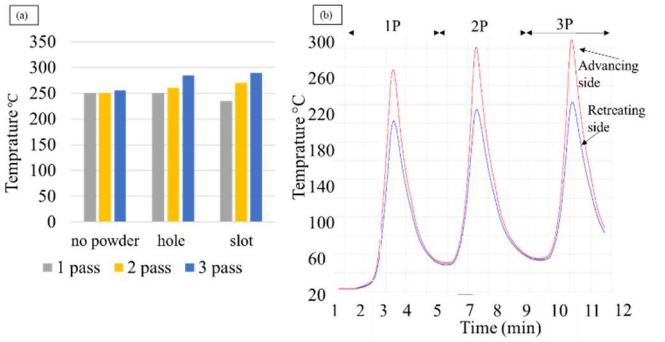

Fig. 10. (a) Temperature comparison at S1100-70 three passes. (b) Temperature profiles for the three passes for sample S1100-70 slot design.

3.5 Power consumption

During the FSW process, the power absorbed has been analyzed and different phases of the process have been highlighted in Figure 11. The power consumption of slot design with powder at one pass, two passes, and three passes have been measured by using a digital multimeter at three different rotational speeds 700, 900, and 1100 rpm while keeping the same traverse speed of 70 mm/min. The initial Power during the positioning phase was between 3000-4000 watts, During the tool plunge phase the power increased rapidly to its maximum value in between 5000-6000 watts. The temperature starts increasing and the material plasticizes. With the increase of temperature and deformation of the material, the welding process starts, and power continuously decreases to its minimum power consumption value. The same trend was observed for all three passes. The results reveal that with the increment of tool rotational speed, the power consumption also increases and vice versa.

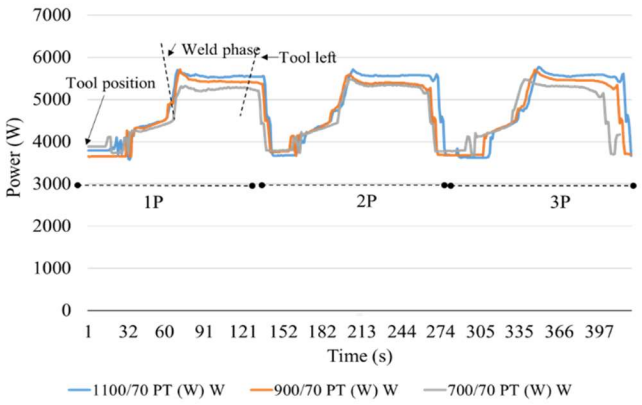

Fig. 11. Power consumption of slot design with powder at S1100-70, S900-70, and S700-70 at three passes.

4. Conclusions

FSW of 2024-T3 aluminum alloy reinforced with micro-sized SiC was carried out in this research. A slot design has been proposed to integrate the micro SiC seamlessly into the FSW process without any loss. The comparison has been made with the hole plate and no-powder joints in order to highlight the effect of plate design and powder. The entire process has been carried out with three passes. It was found that, by adding powder through the proposed slot design, the local mechanical properties of the welded joints are improved due to the dynamic recrystallization and pinning mechanisms, while the agglomeration of SiC particles within the stir zone (SZ) negatively impacts the weld joints. The following conclusion can be drawn from the results.

- Sound welds can be produced both with SiC powder and without powder using proper process parameters.
- The new slot design proposed can successfully address the issue of powder dispersal from the welded zone occurring during the process using the conventional hole configuration.
- The maximum hardness obtained in slot plates was 178 HV, which is 30 % higher than the base material hardness.
- The UTS of slot designed welded joints decreases due to the agglomeration of SiC, exacerbating the stress concentration prone to fracture under tensile loads.
- The inclusion of SiC in the stir zone has been found to impede grain growth as a result of its pinning effect, thereby leading to a reduction in grain size.
- Homogenous dispersion of SiC were observed at S-1100-70 in both slot design and hole design welded plate, which exhibits good mechanical and microstructural properties in comparison with other process parameters.
- The slot design of the welded joints exhibits a higher volume fraction of SiC compared to the hole design.
- The power consumption increases with an increase in rotational speed, while the change in traverse speed does not have any significant effect on power consumption.
- Temperature increases with the increase in the number of passes in reinforced welded joints due to the uniform distribution of SiC.

Future work will be focused on the wear resistance enabled in the reinforced welds as a function of the joint design.

Fundings

This study was carried out within the MICS (Made in Italy – Circular and Sustainable) Extended Partnership and received funding from the European Union Next-Generation EU (PIANO NAZIONALE DI RIPRESA E RESILIENZA (PNRR) – MISSIONE 4 COMPONENTE 2, INVESTIMENTO 1.3 – D.D. 1551.11–10-2022, PE00000004). This manuscript reflects only the authors' views and opinions, neither the European Union nor the European Commission can be considered responsible for them.

References

[1] D. Yadav, R. Bauri, A. Kauffmann, and J. Freudenberger, "Al-Ti Particulate Composite: Processing and Studies on Particle Twinning, Microstructure, and Thermal Stability," *Metall Mater Trans A Phys Metall Mater Sci*, vol. 47, no. 8, pp. 4226–4238, Aug. 2016, doi: 10.1007/s11661-016-3597-1.

[2] M. M. Moradi, H. Jamshidi Aval, and R. Jamaati, "Effect of pre and post welding heat treatment in SiC-fortified dissimilar AA6061-AA2024 FSW butt joint," *J Manuf Process*, vol. 30, pp. 97–105, Dec. 2017, doi: 10.1016/j.jmapro.2017.08.014.

[3] R. S. Mishra and Z. Y. Ma, "Friction stir welding and processing," *Materials Science and Engineering R: Reports*, vol. 50, no. 1–2. Aug. 31, 2005. doi: 10.1016/j.mser.2005.07.001.

[4] P. L. Threadgilll, A. J. Leonard, H. R. Shercliff, and P. J. Withers, "Friction stir welding of aluminium alloys," *International Materials Reviews*, vol. 54, no. 2. Maney Publishing, pp. 49–93, 2009. doi: 10.1179/174328009X411136.

[5] M. W. Safeen, P. Russo Spena, G. Buffa, D. Campanella, A. Masnata, and L. Fratini, "Effect of position and force tool control in friction stir welding of dissimilar aluminum-steel lap joints for automotive applications," *Adv Manuf*, vol. 8, no. 1, pp. 59–71, Mar. 2020, doi: 10.1007/s40436-019-00290-1.

[6] N. Vidakis, N. Mountakis, A. Moutsopoulou, C. David, N. K. Nasikas, and M. Petousis, "The impact of process parameters and pin-to-shoulder diameter ratio on the welding performance of polycarbonate in FSW," *International Journal of Advanced Manufacturing Technology*, 2023, doi: 10.1007/S00170-023-12192-5.

[7] H. Uzun, "Friction stir welding of SiC particulate reinforced AA2124 aluminium alloy matrix composite," *Mater Des*, vol. 28, no. 5, pp. 1440–1446, 2007, doi: 10.1016/j.matdes.2006.03.023.

[8] A. Heidarzadeh *et al.*, "Friction stir welding/processing of metals and alloys: A

comprehensive review on microstructural evolution," *Progress in Materials Science*, vol. 117. Elsevier Ltd, Apr. 01, 2021. doi: 10.1016/j.pmatsci.2020.100752.

[9] N. Saini, C. Pandey, S. Thapliyal, and D. K. Dwivedi, "Mechanical Properties and Wear Behavior of Zn and MoS2 Reinforced Surface Composite Al- Si Alloys Using Friction Stir Processing," *Silicon*, vol. 10, no. 5, pp. 1979–1990, Sep. 2018, doi: 10.1007/s12633-017-9710-2.

[10] S. S. Mirjavadi *et al.*, "Influence of TiO2 nanoparticles incorporation to friction stir welded 5083 aluminum alloy on the microstructure, mechanical properties and wear resistance," *J Alloys Compd*, vol. 712, pp. 795–803, 2017, doi: 10.1016/j.jallcom.2017.04.114.

[11] L. M. Marzoli, A. V. Strombeck, J. F. Dos Santos, C. Gambaro, and L. M. Volpone, "Friction stir welding of an AA6061/Al2O3/20p reinforced alloy," *Compos Sci Technol*, vol. 66, no. 2, pp. 363–371, Feb. 2006, doi: 10.1016/j.compscitech.2005.04.048.

[12] J. P. Chen, L. Gu, and G. J. He, "A review on conventional and nonconventional machining of SiC particle-reinforced aluminium matrix composites," *Advances in Manufacturing*, vol. 8, no. 3. Shanghai University, pp. 279–315, Sep. 01, 2020. doi: 10.1007/s40436-020-00313-2.

[13] A. Dolatkhah, P. Golbabaei, M. K. Besharati Givi, and F. Molaiekiya, "Investigating effects of process parameters on microstructural and mechanical properties of Al5052/SiC metal matrix composite fabricated via friction stir processing," *Mater Des*, vol. 37, pp. 458–464, May 2012, doi: 10.1016/j.matdes.2011.09.035.

[14] M. Bahrami, K. Dehghani, and M. K. Besharati Givi, "A novel approach to develop aluminum matrix nano-composite employing friction stir welding technique," *Mater Des*, vol. 53, pp. 217–225, 2014, doi: 10.1016/j.matdes.2013.07.006.

[15] M. Bahrami, N. Helmi, K. Dehghani, and M. K. B. Givi, "Exploring the effects of SiC reinforcement incorporation on mechanical properties of friction stir welded 7075 aluminum alloy: Fatigue life, impact energy, tensile strength," *Materials Science and Engineering A*, vol. 595, pp. 173–178, Feb. 2014, doi: 10.1016/j.msea.2013.11.068.

[16] N. Vidakis, M. Petousis, N. Mountakis, and J. D. Kechagias, "Optimization of friction stir welding for various tool pin geometries: the weldability of Polyamide 6 plates made of material extrusion additive manufacturing," *International Journal of Advanced Manufacturing Technology*, vol. 124, no. 7–8, pp. 2931–2955, Feb. 2023, doi: 10.1007/s00170-022-10675-5.

[17] A. Vairis, G. Papazafeiropoulos, and A. M. Tsainis, "A comparison between friction stir welding, linear friction welding and rotary friction welding," *Adv Manuf*, vol. 4, no. 4, pp. 296–304, Dec. 2016, doi: 10.1007/s40436-016-0163-4.

[18] S. K. Dewangan, P. N. Banjare, M. K. Tripathi, and M. K. Manoj, "Effect of vertical and horizontal zinc interlayer on material flow, microstructure, and mechanical properties of dissimilar FSW of Al 7075 and Mg AZ31 alloys," *International Journal of Advanced Manufacturing Technology*, vol. 126, no. 9–10, pp. 4453–4474, Jun. 2023, doi: 10.1007/s00170-023-11348-7.

[19] G. Buffa, M. De Lisi, E. Sciortino, and L. Fratini, "Dissimilar titanium/aluminum friction stir welding lap joints by experiments and numerical simulation," *Adv Manuf*, vol. 4, no. 4, pp. 287–295, Dec. 2016, doi: 10.1007/s40436-016-0157-2.

[20] M. Abbasi Gharacheh, A. H. Kokabi, G. H. Daneshi, B. Shalchi, and R. Sarrafi, "The influence of the ratio of 'rotational speed/traverse speed' (ω/v) on mechanical properties of AZ31 friction stir welds," *Int J Mach Tools Manuf*, vol. 46, no. 15, pp. 1983–1987, Dec. 2006, doi: 10.1016/j.ijmachtools.2006.01.007.

[21] D. Khayyamin, A. Mostafapour, and R. Keshmiri, "The effect of process parameters on microstructural characteristics of AZ91/SiO 2 composite fabricated by FSP," *Materials Science and Engineering A*, vol. 559, pp. 217–221, Jan. 2013, doi: 10.1016/j.msea.2012.08.084.

[22] M. Barmouz and M. K. B. Givi, "Fabrication of in situ Cu/SiC composites using multi-pass friction stir processing: Evaluation of microstructural, porosity, mechanical and electrical behavior," *Compos Part A Appl Sci Manuf*, vol. 42, no. 10, pp. 1445–1453, Oct. 2011, doi: 10.1016/j.compositesa.2011.06.010.

[23] M. Zohoor, M. K. Besharati Givi, and P. Salami, "Effect of processing parameters on fabrication of Al-Mg/Cu composites via friction stir processing," *Mater Des*, vol. 39, pp. 358–365, Aug. 2012, doi: 10.1016/j.matdes.2012.02.042.

[24] T. Singh, S. K. Tiwari, and D. K. Shukla, "Mechanical and microstructural characterization of friction stir welded AA6061-T6 joints reinforced with nano-sized particles," *Mater Charact*, vol. 159, Jan. 2020, doi: 10.1016/j.matchar.2019.110047.

[25] N. Sharifi Asl, S. E. Mirsalehi, and K. Dehghani, "Effect of TiO 2 nanoparticles addition on microstructure and mechanical properties of dissimilar friction stir welded AA6063-T4 aluminum alloy and AZ31B-O magnesium alloy," *J Manuf Process*, vol. 38, pp. 338–354, Feb. 2019, doi: 10.1016/j.jmapro.2019.01.023.

[26] J. Gandra, R. Miranda, P. Vilaa, A. Velhinho, and J. P. Teixeira, "Functionally graded materials produced by friction stir processing," *J Mater Process Technol*, vol. 211, no. 11, pp. 1659–1668, 2011, doi: 10.1016/j.jmatprotec.2011.04.016.

[27] A. Sharma, V. M. Sharma, S. Mewar, S. K. Pal, and J. Paul, "Friction stir processing of Al6061-SiC-graphite hybrid surface composites," *Materials and Manufacturing Processes*, vol. 33, no. 7, pp. 795–804, May 2018, doi: 10.1080/10426914.2017.1401726.

[28] J. Guo, B. Y. Lee, Z. Du, G. Bi, M. J. Tan, and J. Wei, "Effect of Nano-Particle Addition on Grain Structure Evolution of Friction Stir-Processed Al 6061 During Postweld Annealing," *JOM*, vol. 68, no. 8, pp. 2268–2273, Aug. 2016, doi: 10.1007/s11837-016-1991-1.

[29] M. Zehsaz, S. Hassanifard, and F. Esmaeili, "Fatigue life estimation for different notched specimens based on the volumetric approach," in *EPJ Web of*

Conferences, EDP Sciences, Jun. 2010. doi: 10.1051/epjconf/20100642001.

[30] C. Pandey, M. M. Mahapatra, P. Kumar, F. Daniel, and B. Adhithan, "Softening mechanism of P91 steel weldments using heat treatments," *Archives of Civil and Mechanical Engineering*, vol. 19, no. 2, pp. 297–310, Mar. 2019, doi: 10.1016/j.acme.2018.10.005.